THE JOURNAL OF PHYSICAL CHEMISTRY Letters

pubs.acs.org/JPCL Letter

Control of Charge Carrier Dynamics in Plasmonic Au Films by TiO_x Substrate Stoichiometry

Teng-Fei Lu, Yi-Siang Wang, John A. Tomko, Patrick E. Hopkins, Hong-Xing Zhang,* and Oleg V. Prezhdo*

Cite This: *J. Phys. Chem. Lett.* 2020, 11, 1419−1427 Read Online

ACCESS | Metrics & More | Article Recommendations | Supporting Information

ABSTRACT: Plasmonic excitations in noble metals have many fascinating properties and give rise to a broad range of applications. We demonstrate, using nonadiabatic molecular dynamics combined with time-domain density functional theory, that the chemical composition and stoichiometry of substrates can have a strong influence on charge dynamics. By changing oxygen content in TiO_2, including stoichiometric, oxygen rich, and oxygen poor phases, and Ti metal, one can alter lifetimes of charge carriers in Au by a factor of 5 and control the ratio of electron-to-hole relaxation rates by a factor of 10. Remarkably, a thin TiO_x substrate greatly alters charge carrier properties in much thicker Au films. Such large variations stem from the fact that the Ti and O atoms are much lighter than Au, and their vibrations are much faster at dissipating the energy. The control over a particular charge carrier and an energy range depends on the Au and TiO_x level alignment, and the interfacial interaction strength. These factors are easily influenced by the TiO_x stoichiometry. In particular, oxygen rich and poor TiO_2 can be used to control holes and electrons, respectively, while metallic Ti affects both charge carriers. The detailed atomistic analysis of the interfacial and electron-vibrational interactions generates the fundamental understanding of the properties of plasmonic materials needed to design photovoltaic, photocatalytic, optoelectronic, sensing, nanomedical, and other devices.

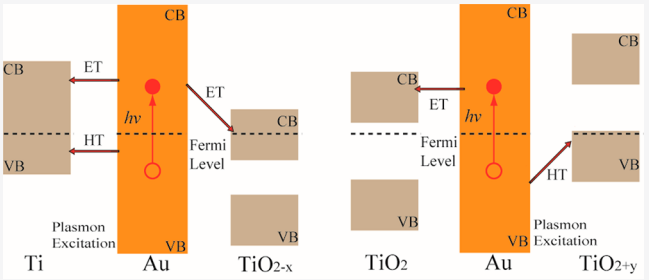

Localized surface plasmon resonance (LSPR) of Au and other noble metal particles has attracted great interest due to its fascinating optical and electronic properties, which give rise to a wide range of applications in solar energy harvesting, catalysis, optoelectronics, nanomedicine, microelectronic thermal management, biosensing, etc.[1−6] LSPR stems from a resonant interaction between electromagnetic waves and conduction band electrons in metals.[7] The LSPR frequency is strongly sensitive to shape, size, geometry, and composition of the nanoparticle and is governed primarily by the free electron density of the material, adjusted by its high frequency dielectric constant.[8,9] Control of the electron density on the nanoparticle surface, provided by composition and geometry allows one to manipulate absorption and scattering of light.[10−12]

By exciting the LSPR in noble metal nanoparticles with ultrafast pulsed laser irradiation, one can efficiently convert light into heat. The nontrivial electron−phonon dynamics and heating led to spectral broadening of the surface plasmon absorption. The rapid electron-vibrational relaxation generates thermal energy that lends itself toward applications such as photothermal therapy.[13−16] However, this electron−phonon relaxation should be avoided in photovoltaic and optical data storage devices, as the relaxation leads to unfavorable energy losses.[17]

The electron−phonon energy transfer and relaxation are often described by the two-temperature model (TTM),[18,19] in which electrons and phonons are assigned different effective temperatures, T_e and T_p, and an electron−phonon coupling constant, G, governs energy transport between the two subsystems. Typically, electrons are excited to a hotter temperature and transfer energy to the colder phonons. Ultimately, the two subsystems equilibrate to the same temperature on a time scale determined by the electron−phonon coupling factor. The TTM provides a straightforward and very useful description of the nonequilibrium electron-vibrational dynamics, but it has its limitations. Rigorously, the concept of temperature applies only to systems' thermodynamic equilibrium. One can define separate and time-dependent electron and phonon temperatures, because electrons evolve much faster than phonons and equilibrate by electron−electron scattering on time scales significantly shorter than electron-vibrational energy exchange. More complicated descriptions consider an energy-dependent

Received: December 30, 2019
Accepted: February 3, 2020
Published: February 3, 2020

Downloaded via UNIV OF VIRGINIA on March 19, 2020 at 02:18:01 (UTC).
See https://pubs.acs.org/sharingguidelines for options on how to legitimately share published articles.

ACS Publications © 2020 American Chemical Society

electron−phonon coupling constant, $G(E)$, which depends on density of electronic states, or solve quantum master or Schrodinger equations.[20] Pulsed laser measurement techniques are often used to study electron-vibrational energy exchange and other nonequilibrium processes.[21,22]

The ability to adjust carrier concentration in metal particles constitutes an important tool to tune the optical response, in particular, the frequency of the collective plasmon oscillation.[23,24] The LSRP of metal nanoparticles can be tuned by chemical composition or changes in geometry during nanoparticle synthesis. Changes in the carrier concentration can be used to tune the LSRP response dynamically, as demonstrated by Garcia et al. with doped semiconductor nanocrystals.[25]

Substrates are commonly used to assemble nanoparticles into more complex nanostructures, in order to achieve advanced optical and electronic functionalities.[26,27] Often, the substrates play active roles, modifying material's optical and electronic response. Giri et al. reported that Ti adhesion layers, which are used to improve interface bonding between an Au layer and various dielectric materials, enhance electron-vibrational interactions, and accelerate energy exchange.[28] Wang et al. demonstrated that anatase TiO_2 nanosheets sensitized with Au nanoparticles show a significantly improved photoresponse at the LSPR wavelength, enhancing the photocatalytic reduction efficiency.[29] Defects, such as oxygen vacancies, are common in TiO_2, and can be used to adjust its electronic and optical proprieties.[30,31] Olson et al. demonstrated that the oxygen stoichiometry of the TiO_x layer has a significant influence on the thermal boundary conductance at Au/TiO_x/dielectric interfaces.[32] Kumar et al. used non-stoichiometric plasmonic Au/TiO_x nanocomposites to improve photocatalytic activity and utilization of the solar light spectrum.[33]

In this work, we demonstrate how the stoichiometry of a TiO_x substrate can be used to control dynamics of excited charge carriers at Au/TiO_x interfaces and to rationalize why different substrate compositions strongly influence charge carrier relaxation. By considering a pristine Au film, and an Au film interfaced with metallic Ti, stoichiometric TiO_2, and oxygen rich and deficient TiO_2, we show that the influence of the TiO_x substrates on the properties of charge carriers inside the Au film depends on interfacial interactions and alignment of the Au and TiO_x energy levels. Provided a good interfacial contact and proper level alignment are achieved, Au wave functions delocalize onto TiO_x. Because the Ti and O atoms are much lighter than the Au atoms, charges move to the TiO_x substrate and deposit their energy into TiO_x phonons. Hole dynamics are faster and more important than dynamics of electrons, and photoexcitation energy is deposited primarily into holes, because holes are supported by a much denser state manifold. However, by tuning the TiO_x substrate stoichiometry, one can make electron and hole dynamics symmetric. Overall, TiO_x can alter the absolute values of the charge−phonon relaxation rate by a factor of 5, and the electron-to-hole relaxation rate ratio by a factor of 10. Holes are influenced by oxygen rich TiO_2 substrates, while electrons are affected by oxygen deficient TiO_2, as determined by the energy level alignment. This study shows that the interfacial Au/TiO_x interactions are enhanced for nonstoichiometric TiO_x, compared to the case of perfect TiO_2. The fundamental principles uncovered by the presented theoretical study apply to other metal/semiconductor and metal/metal interfaces and provide a framework for understanding and designing novel nanoscale materials for a broad range of applications.

The charge carrier relaxation dynamics are simulated using nonadiabatic molecular dynamics (NAMD).[34−38] NAMD is a mixed quantum-classical technique that treats the heavier nuclei classically, while maintaining a quantum-mechanical description of the lighter electrons. The NAMD simulations are performed using the fewest switching surface hopping (FSSH) algorithm,[39] which is one of the most popular and efficient approaches. It is suitable for studying processes in which electronic transitions happen faster than phonon-induced loss of coherence within the electronic subsystem, including intraband charge−phonon relaxation. Transitions taking a long time, such as charge trapping by midgap states and recombination in semiconductors, require inclusion of decoherence effects, provided for instance by decoherence-induced surface hopping.[40] FSSH can be viewed as a first-order theory, and it has been generalized with global flux surface hopping[41] to include higher order superexchange and many particle processes.[42,43] The NAMD methodology is formulated within real-time time-dependent density functional theory (TDDFT) in the Kohn−Sham framework[44] and implemented in the PYthon eXtension for Ab Initio Dynamics (PYXAID) package,[45,46] under the classical path approximation, which allows for substantial computational savings. A description of the theoretical methodology and the computational details are provided in the Supporting Information. The methodology has been successfully utilized to describe excited state dynamics in a wide variety of nanoscale and condensed matter systems.[46−58]

In order to investigate the influence of the TiO_x stoichiometry on the electron−phonon dynamics, we select the following five systems (Figure 1). The seven-layer pure Au

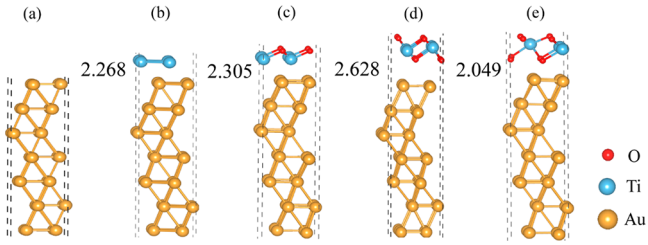

Figure 1. Geometries of (a) pure Au(111) slab, and Au(111) slab with absorbed (b) Ti, (c) Ti_4O_4, (d) Ti_4O_8 and (e) Ti_3O_8 layers at 0 K. The numbers on the left side of the structures indicate the distances between the TiO_x layer and the nearest Au layer.

slab and the Au slab covered with a Ti monolayer are selected as references. The Au slab covered with a Ti_4O_8 monolayer represents interaction with stoichiometric titanium dioxide. The oxygen-rich variation of TiO_x is represented by a Ti_3O_8 layer, and an oxygen-deficient TiO_x is represented by Ti_4O_4. These systems are used to perform the quantum dynamics calculations. Additionally, we investigated structures and densities of states (DOS) of systems with thicker TiO_x and Au slabs, Figures S3−S6 of the Supporting Information. As shown in Figure 1, the interaction between the Au slab and the stoichiometric Ti_4O_8 substrate is purely van der Waals and thus weak. The distance between the top Au layer and Ti_4O_8 is 2.628 Å. In comparison, the distances between the top Au layer and the nonstoichiometric Ti_4O_4 and Ti_3O_8 are reduced, 2.305 and 2.049 Å, respectively, indicating that the Au/TiO_x

https://dx.doi.org/10.1021/acs.jpclett.9b03884
J. Phys. Chem. Lett. 2020, 11, 1419−1427

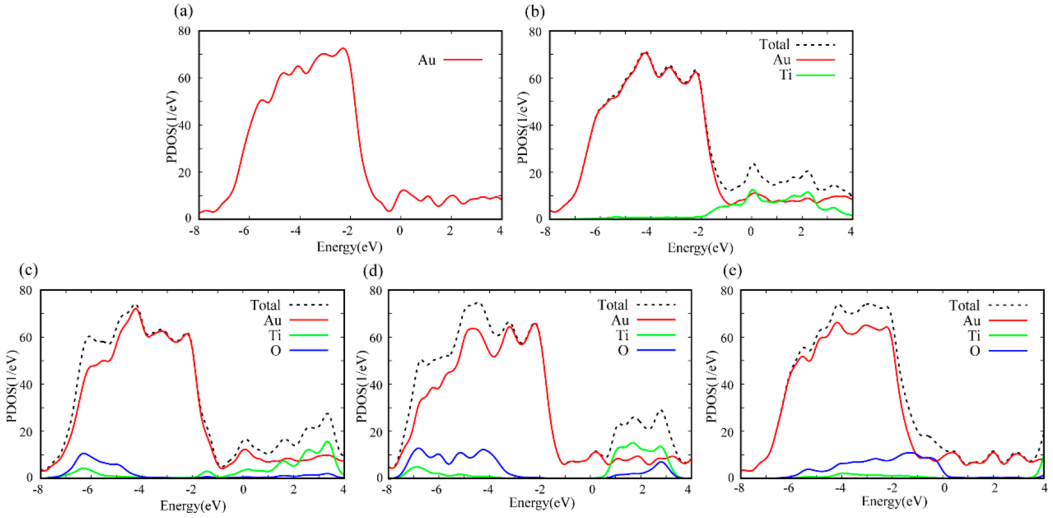

Figure 2. Projected density of states (PDOS) of (a) Au, (b) Au/Ti, (c) Au/Ti_4O_4, (d) Au/Ti_4O_8, and (e) Au/Ti_3O_8 for the optimized ground-state structure. The Fermi levels are set to 0 eV.

interactions become stronger for nonstoichiometric titanium dioxide. It has been computationally demonstrated that an increased strength of interfacial atomic interactions can change phonon-driven thermal transport across interfaces.[59] One can expect a similar effect for electron−phonon energy transport. In this case, however, the energy transfer depends not only on the strength of interfacial interactions but also on the relative alignment of electronic energy levels of the two subsystems. TiO_2 is a semiconductor and can contribute to the electron−phonon energy exchange only if it has electronic levels within the relevant energy range.

The dependence of the electronic structure of the Au/TiO_x interfaces on the TiO_x stoichiometry can be understood by considering the density of states (DOS), as shown in Figure 2. The total DOS is split into the contributions from the Au (red line), Ti (green line), and O (blue line) atoms. The Fermi level defines the zero energy. Shown in Figures S5 and S6 of the Supporting Information, the DOS of thicker Au slabs, as well as of Au/TiO_x interfaces with thicker TiO_x slabs are similar to the DOS shown in Figure 2. In particular, the alignment of the TiO_x levels with respect to the Fermi energy of the Au slab depend on whether TiO_x is stoichiometric, O-rich or Ti-rich, rather than on the TiO_x slab thickness. The DOS of the Au slab undergoes a sharp drop in the energy range from −2 to −1 eV, Figure 2a. The thicker Au leads to a growth in the contribution of DOS due to the increase in Au atoms. Considering the Au/Ti system, Figure 2b, we observe an increase in the Ti partial DOS (pDOS) within the same energy range, in agreement with previous calculations.[60] Notably, the pDOS of the Ti monolayer is the same as the pDOS of the seven-layer Au slab at energies about −1 eV, indicating that Ti contributes many more states per atom than Au, around and above the Fermi energy.

The pure Au and Au/Ti systems are fully metallic, with the Ti substrate contributing states at the Fermi energy. In contrast, the TiO_x substrate in the Au/TiO_x interfaces is a semiconductor and contains a large gap in its electronic energy spectrum. The Fermi energy in the Au/TiO_x systems is controlled by Au. Notably, the alignment of the TiO_x bandgap relative to the Au Fermi energy is strongly dependent on the TiO_x stoichiometry. Generally, the TiO_x valence band (VB) is formed by O atomic orbitals, while the conduction band (CB) arises from Ti atomic orbitals. Defects in TiO_2 can be regarded as dopants that shift the TiO_2 Fermi level. Such intrinsic doping influences alignment of the Au and TiO_x Fermi levels. Specifically, the Ti-rich Ti_4O_4 can be viewed as either Ti-doped TiO_2 or as TiO_2 with O vacancies. In this case, the TiO_2 CB contains electrons; i.e., the TiO_2 Fermi energy moves to the CB, and the Ti_4O_4 bandgap resides below the Au Fermi energy, Figure 2c. In contrast, the O-rich Ti_3O_8 is missing electrons in the VB, because the extra O atoms did not receive electrons from Ti. As a result, the Ti_3O_8 Fermi level resides in the VB and the Ti_3O_8 bandgap is above the Au Fermi level.

Photon absorption by the Au slab generates both electrons and holes. The large asymmetry in the Au DOS above and below the Fermi level, Figure 2, indicates that most of the photon energy is deposited into holes rather than electrons, because statistically the number of excitation from deep hole levels into shallow electron levels is larger than the number of excitation from shallow hole levels to deep electron levels.[23,24] Therefore, the hole relaxation largely decides the time scale observed in experiments. The DOS of pure Au suggests that holes should relax faster than electrons, because the hole DOS is larger. However, as holes approach the Fermi energy, relaxing from −1 to 0 eV, they should slow down significantly. By introducing electronic states at −1 eV and above, Figure 2b, the Ti adhesion layer should accelerate both electron relaxation and hole relaxation close to the Fermi energy.

Considering the alignment of the pDOS of the TiO_x substrates with the Au pDOS, one can anticipate that stoichiometric TiO_2 should accelerate the electron relaxation without influencing the holes too much, Figure 2d. The Ti-rich Ti_4O_4 introduces states both above and below the Fermi level, Figure 2c, and therefore, it should accelerate relaxation of both electrons and holes, but mostly electrons. In contrast, the O-rich Ti_3O_8 should influence hole relaxation, but not electron relaxation, Figure 2e. Similar conclusions can be drawn from the thicker Ti-rich and O-rich TiO_x slabs, Figure S6. The pDOS analysis does not provide a complete picture, because the electron−phonon relaxation depends on other factors as well, most notably on the velocity of the nuclei that couple to the electronic subsystem. Note the nonadiabatic coupling (NAC) dependence on the nuclear velocity, eq S5 of the Supporting Information. Thus, even if TiO_x has no electronic

https://dx.doi.org/10.1021/acs.jpclett.9b03884
J. Phys. Chem. Lett. 2020, 11, 1419−1427

states within a certain energy range, it can still accelerate the relaxation if the much lighter Ti and especially O atoms couple to the heavy Au atoms and introduce fast, high frequency vibrations.

The hot carrier relaxation is governed by electron−phonon coupling, which in the NAMD simulation is reflected in the NAC. The NAC matrix element, eq S5, depends on overlap of initial and final wave functions, motivating one to investigate wave function delocalization between the Au and TiO_x subsystems. Figure 3 depicts distributions of averaged charge densities for hole states over several energy ranges below the Fermi energy. The corresponding data for electron states are shown in Figure S1. The charge density distributions in the Au/TiO_x interfaces is a good match to the pDOS, Figure 2. We focus on the holes, because photons absorbed by Au deposit most of their energy into holes rather than electrons, due to the higher hole DOS.[61] Figure 3 shows that the wave functions of the pure Au film are symmetric and are distributed either within the core or surface regions of the slabs as the energy changes. The charge densities of the Au/Ti system are delocalized inside Au at energies below −2 eV. At energies above −2 eV, the Au wave functions can strongly hybridize with the Ti substrate, Figure 3b, matching the decrease of the Au pDOS and increase of the Ti pDOS, Figure 2b.

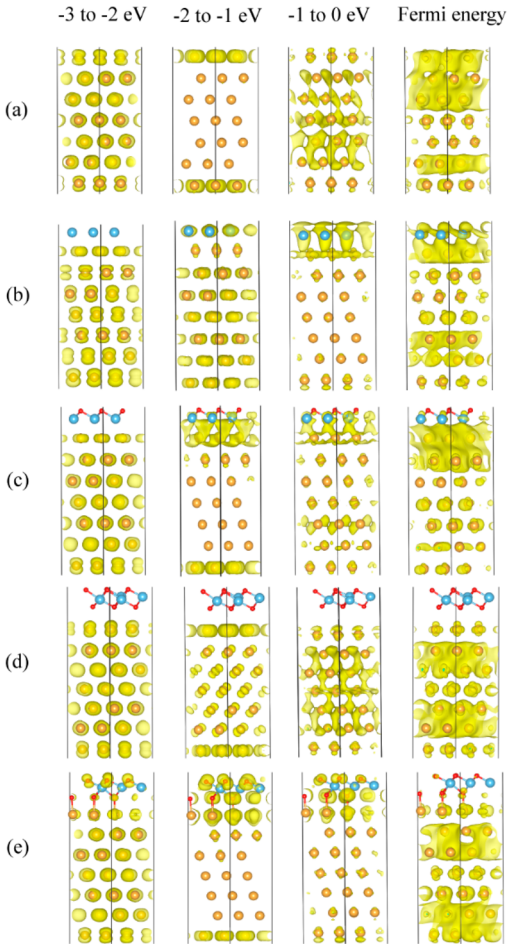

Figure 3. Charge densities of the electronic state at the Fermi energy and average charge densities within energy ranges from −3 to −2 eV, −2 to −1 eV, and −1 to 0 eV for (a) Au, (b) Au/Ti, (c) Au/Ti_4O_4, (d) Au/Ti_4O_8, and (e) Au/Ti_3O_8. The results for states above the Fermi energy are shown in Figure S1.

The electronic coupling between Au and perfect Ti_4O_8 is very weak below the Fermi energy, because the Ti_4O_8 bandgap is located in this energy window, Figure 2d. As a result, the hole charge densities are localized entirely on the Au slab. However, significant mixing between the Au and TiO_x states is seen in the nonstoichiometric TiO_x systems. The state mixing is less pronounced for Au/Ti_4O_4 than Au/Ti_3O_8, because Ti_3O_8 has higher pDOS below the Fermi energy. The charge density trends are quite different above the Fermi energy, Figure S1, compared to the energies below the Fermi level, Figure 3. In particular, the Ti_4O_8 and Ti_3O_8 systems show the opposite trends for electrons and holes.

Generally, the TiO_x stoichiometry at the Au/TiO_x interfaces has a strong influence on both the DOS, Figure 2, and the orbital localization, Figure 3. Because the TiO_x substrates are composed of much lighter atoms than the Au slab, and since the NAC depends on the nuclear velocity, eq S5, one can expect that mixing of Au wave functions with TiO_x states should modify the charge relaxation dynamics.

We consider nonradiative electron and hole relaxation dynamics starting at energies around 3.1 eV away from the Fermi energy. Such excitation energy corresponds to the violet/near UV part of the solar spectrum, representing the higher end of the energies harvested in solar applications. Thus, the simulated charge relaxation covers the whole energy range encountered in solar energy applications. The electronic relaxation occurs by coupling to phonons, and the light energy is converted into electronic energy and then heat.[62] Figure 4 presents the energy relaxation curves for both holes and electrons. Table 1 reports the hole and electron relaxation time scales obtained through exponential fitting of the data. The hole relaxation is faster than the electron relaxation in all systems, because of the higher hole DOS, Figure 2. Compared to results for pure Au, the hole relaxation is accelerated by all substrates, except for the stoichiometric Ti_4O_8, Figure 4a, because Ti_4O_8 has no states below the Fermi level. The hole is accelerated most by Ti_3O_8, because the O-rich system pins the TiO_x VB edge to the Au Fermi energy and introduces many new states below the Fermi level. Even though the relative contribution of the narrow Ti_3O_8 layer to the overall DOS is small, compared to the contribution to the Au pDOS, Ti_3O_8 has a strong influence on the charge−phonon relaxation dynamics, because O and Ti atoms are much lighter than Au. The trend is reversed for the electron relaxation, Figure 4b. The O-rich Ti_3O_8 substrate has no influence on the electron relaxation, because the Ti_3O_8 layer has the bandgap in that energy range.

The TiO_x stoichiometry can change the ratio of the electron and hole relaxation rates. Although in most systems holes relax much faster than electrons due to the higher hole DOS, Figure 2, electrons relax at the same rate as holes in Au/Ti_4O_4, Figure 4 and Table 1. Overall, changes in the TiO_x stoichiometry can have very pronounced effects on both absolute and relative values of the charge−phonon relaxation rates. The narrow O-rich Ti_3O_8 substrate layer accelerates hole relaxation by a factor of 4.5 relative to pristine Au. The ratio of hole-to-electron relaxation rates changes from 1 for Ti_4O_4 to 10 in Ti_3O_8. Interestingly, the semiconducting Ti_3O_8 accelerates hole relaxation in the Au slab more than the metallic Ti_4. This is because the former contains O atoms, which are much lighter

https://dx.doi.org/10.1021/acs.jpclett.9b03884
J. Phys. Chem. Lett. 2020, 11, 1419−1427

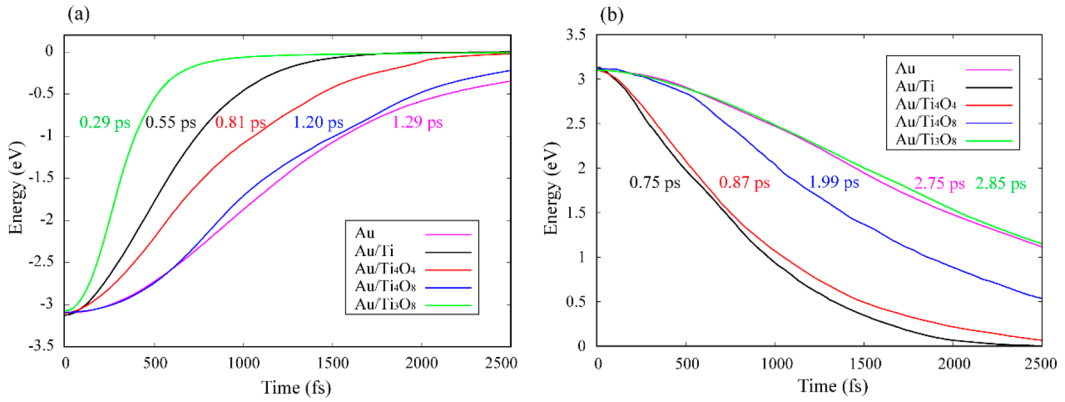

Figure 4. Energy decay of (a) hole and (b) electron in investigated systems. Holes relax faster than electrons because of the higher DOS, Figure 2. The decay time shows strong dependence on the TiO_x layer stoichiometry, which determines at what energies TiO_x contributes to the DOS, Figure 2.

Table 1. Absolute Value of Nonadiabatic Coupling Averaged over Different Energy Ranges and Hole and Electron Relaxation Times, τ, in the Five Systems at 300 K

	hole relaxation					electron relaxation				
	0 to −1 eV	−1 to −2 eV	−2 to −3 eV	0 to −3 eV	τ ps	0 to 1 eV	1 to 2 eV	2 to 3 eV	0 to 3 eV	τ ps
Au	1.49	0.48	1.12	1.25	1.29	2.29	0.49	1.10	1.21	2.75
Au/Ti	2.04	2.62	2.85	1.75	0.55	2.33	2.77	2.57	1.41	0.75
Au/Ti_4O_4	2.85	1.42	1.33	1.33	0.81	1.56	1.07	1.89	1.32	0.87
Au/Ti_4O_8	1.40	0.45	1.88	1.30	1.20	2.56	1.62	1.09	1.24	1.88
Au/Ti_3O_8	1.18	6.68	3.14	2.72	0.29	1.22	0.98	1.60	1.19	2.85

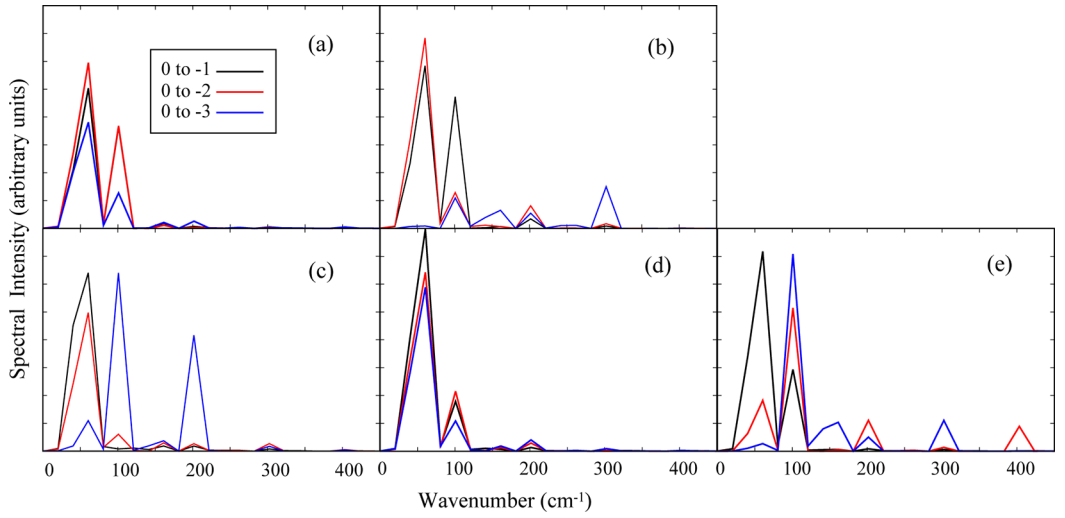

Figure 5. Phonon influence spectra of the energy gaps from the Fermi level to the electronic levels at −1, −2, and −3 eV below it for the hole relaxation in (a) Au, (b) Au/Ti, (c) Au/Ti_4O_4, (d) Au/Ti_4O_8, and (e) Au/Ti_3O_8. The corresponding results for the electron relaxation are shown in Figure S2.

than both Ti and Au and has states in the relevant energy range.

The NAMD simulations show that stoichiometry of the TiO_x substrate is a very powerful tool for controlling the charge−phonon relaxation behavior. The stoichiometry can be used to influence lifetimes of hot charge carriers and to determine which carriers, positive or negative, live longer.

In order to provide further insights into the origin of the strong dependence of the charge−phonon relaxation rates on the TiO_x substrate stoichiometry, we analyze the magnitude of the NAC matrix elements and the frequencies of the phonon modes that couple to the charges. The influence of the substrate stoichiometry on the electronic structure of the Au/TiO_x interfaces is expected to impact the NAC. Table 1 presents the absolute NAC values averaged over electronic states within different energy ranges, covering both the whole span of charge relaxation, and its high, intermediate, and low energy parts. Generally, there is a good correlation between the average absolute NAC value and the relaxation time. The larger the NAC, the faster the relaxation.[63,64] For instance, the hole relaxation is the fastest in Au/Ti_3O_8, and the NAC is the largest. The hole relaxation time scale in pure Au is similar to that in Au/Ti_4O_8, and the NAC values are similar in the two systems.

https://dx.doi.org/10.1021/acs.jpclett.9b03884
J. Phys. Chem. Lett. 2020, 11, 1419−1427

The NAC values exhibit strong energy dependence, indicating that the TTM constitutes a rather crude approximation.[64,65] For example, the NAC in Au/Ti_3O_8, exhibiting the fastest hole relaxation, is the smallest for the 0 to −1 eV energy range, the largest for −1 to −2 eV, and intermediate for −2 to −3 eV. The NAC is large for the energies deep below the Fermi level because of the high Au DOS, Figure 2e. The NAC peaks in the intermediate range from −1 to −2 eV, because the Ti_3O_8 pDOS is highest there. TiO_x has such a strong influence on the NAC because it is composed of light atoms that have large velocities that enter the NAC, eq S5 of the Supporting Information.

To characterize the frequencies of the phonon modes that couple to the charge relaxation, we compute Fourier transforms (FTs) of the energy gaps between the Fermi level and the hole states at −1, −2, and −3 eV below the Fermi level, Figure 5. The corresponding data for electrons are shown in Figure S2. Because electronic energy levels and energy gaps fluctuate as atoms move, the FTs identify the vibrational frequencies that induce these fluctuations. Such FTs are known as the influence spectra, or spectral densities.[66−68] The height of a spectral peak characterizes the strength of the charge−phonon coupling at that particular frequency. In all systems, the spectral densities exhibit strong peaks below 100 cm^{-1}. These frequencies have been assigned to phonon modes of Au atoms.[51,69] The higher frequency peaks, seen in the Au/TiO_x systems, arise from vibrations of the lighter Ti and O atoms. The stoichiometry of the TiO_x substrate can notably change the influence spectra. In particular, the O-rich Ti_3O_8 substrate exhibits significant signals at high frequencies up to 400 cm^{-1}, because it contains the highest fraction of the lightest O atoms. Participation of the high frequency vibrations correlates with the larger relaxation rate. This observation suggests that substrates and adhesion layers containing light chemical elements should be avoided if one desires to keep charge carriers hot, for instance, in photovoltaic and photocatalytic applications. In contrast, strong coupling of noble metal nanoparticles to biomolecules containing light chemical elements is beneficial in photothermal therapy treatments that rely on rapid transfer of photon energy to heat.

To summarize, we have reported a state-of-the-art time-domain ab initio study of charge carrier dynamics in Au films supported by TiO_x substrates with a broad range of stoichiometries. The simulations mimic most directly time-resolved spectroscopic experiments and provide detailed information on the geometric and electronic structure of Au/TiO_x interfaces, the charge−phonon interactions, and the energy relaxation dynamics. Analysis of the simulation results explains why stoichiometry of the TiO_x substrate can have such a strong influence on the properties of charge carriers in Au films. First, the alignment of the fundamental energy gap of TiO_x with respect to the Au Fermi level depends strongly on TiO_x composition. Second, the Au/TiO_x interaction is enhanced when TiO_2 is nonstoichiometric. Third, TiO_x, compared to Au, presents higher frequency phonons because it is composed of much lighter atoms.

Given a proper energy level alignment and a good interfacial contact, Au electronic wave functions delocalize onto TiO_x. Hot charges generated inside Au by photonic excitations move to TiO_x, deposit their energy into TiO_x phonons, and once cooled, move back into the Au film. Because the density of electronic states in Au is highly asymmetric with respect to the Fermi level, the photoexcitation energy is deposited mostly into holes, and holes relax faster than electrons. The substrate can either enhance or diminish this asymmetry by a factor of 10 and change the absolute values of the relaxation rates by a factor of 5. Remarkably, a thin TiO_x substrate can have such a strong influence on the charge carrier properties in much thicker Au films. On the basis of the doping principles, oxygen rich and oxygen deficient TiO_2 influences holes and electrons in Au, respectively. The charge−phonon relaxation times obtained in the simulations show good agreement with the experimental data.

The simulations demonstrate that a narrow TiO_x substrate or a Ti adhesion layer can be more important than the Au film itself. By controlling the imbalance between hot electrons and holes in the Au film using the TiO_x stoichiometry, one can influence hot carrier concentration and steer the system toward hole or electron catalysis. The TiO_x stoichiometry can also be used to shift the plasmon frequency and to tune the optical response, since it allows one to change charge carrier concentration inside Au. By modifying charge−phonon relaxation rates at Au/TiO_x and related interfaces, one can adapt the system for a particular application type. For instance, slow relaxation is favorable for photocatalysis and photovoltaics, while fast response is needed in nanomedical and optoelectronic applications. Shifting the plasmon frequency is important for optical modulation and smart windows. The conclusions obtained in this work apply to other metal/semiconductor and metal/metal composites. The fundamental scientific principles underlying the charge carrier dynamics allow one to greatly expand the range of desirable material properties and to design novel functional materials toward specific applications.

■ ASSOCIATED CONTENT

Supporting Information

The Supporting Information is available free of charge at https://pubs.acs.org/doi/10.1021/acs.jpclett.9b03884.

Theoretical methodology, computational details, charge densities and phonon influence spectra for electron relaxation, and structures and densities of states for systems with thicker TiO_x and Au slabs (PDF)

■ AUTHOR INFORMATION

Corresponding Authors

Hong-Xing Zhang − *Laboratory of Theoretical and Computational Chemistry, Institute of Theoretical Chemistry, Jilin University, Changchun 130023, People's Republic of China;* orcid.org/0000-0001-5334-733X; Email: zhanghx@jlu.edu.cn

Oleg V. Prezhdo − *Department of Chemistry, University of Southern California, Los Angeles, California 90089, United States;* orcid.org/0000-0002-5140-7500; Email: prezhdo@usc.edu

Authors

Teng-Fei Lu − *Laboratory of Theoretical and Computational Chemistry, Institute of Theoretical Chemistry, Jilin University, Changchun 130023, People's Republic of China; Department of Chemistry, University of Southern California, Los Angeles, California 90089, United States*

Yi-Siang Wang − *Department of Chemistry, University of Southern California, Los Angeles, California 90089, United States*

https://dx.doi.org/10.1021/acs.jpclett.9b03884
J. Phys. Chem. Lett. 2020, 11, 1419−1427

John A. Tomko − *Department of Materials Science and Engineering, University of Virginia, Charlottesville, Virginia 22904, United States;* orcid.org/0000-0001-9260-6568

Patrick E. Hopkins − *Department of Materials Science and Engineering, Department of Mechanical and Aerospace Engineering, and Department of Physics, University of Virginia, Charlottesville, Virginia 22904, United States;* orcid.org/0000-0002-3403-743X

Complete contact information is available at: https://pubs.acs.org/10.1021/acs.jpclett.9b03884

Notes

The authors declare no competing financial interest.

■ ACKNOWLEDGMENTS

The research was supported by the US Department of Defense, Multidisciplinary University Research Initiative, grant No. W911NF-16-1-0406. T.F.L acknowledges financial support provided by the China Scholarship Council (CSC) (No. 201806170253) to visit the University of Southern California.

■ REFERENCES

(1) Kawawaki, T.; Zhang, H.; Nishi, H.; Mulvaney, P.; Tatsuma, T. Potential-Scanning Localized Plasmon Sensing with Single and Coupled Gold Nanorods. *J. Phys. Chem. Lett.* **2017**, *8*, 3637−3641.

(2) Gonzalez-Rubio, G.; Diaz-Nunez, P.; Rivera, A.; Prada, A.; Tardajos, G.; Gonzalez-Izquierdo, J.; Banares, L.; Llombart, P.; Macdowell, L. G.; Alcolea Palafox, M.; et al. Femtosecond Laser Reshaping Yields Gold Nanorods with Ultranarrow Surface Plasmon Resonances. *Science* **2017**, *358*, 640−644.

(3) De Silva Indrasekara, A. S.; Shuang, B.; Hollenhorst, F.; Hoener, B. S.; Hoggard, A.; Chen, S.; Villarreal, E.; Cai, Y. Y.; Kisley, L.; Derry, P. J.; et al. Optimization of Spectral and Spatial Conditions to Improve Super-Resolution Imaging of Plasmonic Nanoparticles. *J. Phys. Chem. Lett.* **2017**, *8*, 299−306.

(4) Shen, B.; Linko, V.; Tapio, K.; Pikker, S.; Lemma, T.; Gopinath, A.; Gothelf, K. V.; Kostiainen, M. A.; Toppari, J. J. Plasmonic Nanostructures through DNA-Assisted Lithography. *Science advances* **2018**, *4*, eaap8978.

(5) Zhang, X. Y.; Han, D.; Ma, N.; Gao, R.; Zhu, A.; Guo, S.; Zhang, Y.; Wang, Y.; Yang, J.; Chen, L. Carrier Density-Dependent Localized Surface Plasmon Resonance and Charge Transfer Observed by Controllable Semiconductor Content. *J. Phys. Chem. Lett.* **2018**, *9*, 6047−6051.

(6) Kohntopp, A.; Dittner, M.; Temps, F. Femtosecond Time-Resolved Dynamics of Trans-Azobenzene on Gold Nanoparticles. *J. Phys. Chem. Lett.* **2016**, *7*, 1088−95.

(7) Long, R.; Prezhdo, O. V. Instantaneous Generation of Charge-Separated State on Tio(2) Surface Sensitized with Plasmonic Nanoparticles. *J. Am. Chem. Soc.* **2014**, *136*, 4343−54.

(8) Zhao, W. W.; Tian, C. Y.; Xu, J. J.; Chen, H. Y. The Coupling of Localized Surface Plasmon Resonance-Based Photoelectrochemistry and Nanoparticle Size Effect: Towards Novel Plasmonic Photoelectrochemical Biosensing. *Chem. Commun.* **2012**, *48*, 895−7.

(9) Zhang, Z.; Chen, Z.; Qu, C.; Chen, L. Highly Sensitive Visual Detection of Copper Ions Based on the Shape-Dependent Lspr Spectroscopy of Gold Nanorods. *Langmuir* **2014**, *30*, 3625−30.

(10) Hedley, G. J.; Quarti, C.; Harwell, J.; Prezhdo, O. V.; Beljonne, D.; Samuel, I. D. W. Hot-Hole Cooling Controls the Initial Ultrafast Relaxation in Methylammonium Lead Iodide Perovskite. *Sci. Rep.* **2018**, *8*, 8115.

(11) Chen, L.; Wang, L.; Shuai, Z.; Beljonne, D. Energy Level Alignment and Charge Carrier Mobility in Noncovalently Functionalized Graphene. *J. Phys. Chem. Lett.* **2013**, *4*, 2158−2165.

(12) Ni, Z.; Pi, X.; Zhou, S.; Nozaki, T.; Grandidier, B.; Yang, D. Size-Dependent Structures and Optical Absorption of Boron-Hyperdoped Silicon Nanocrystals. *Adv. Opt. Mater.* **2016**, *4*, 700−707.

(13) Renero-Lecuna, C.; Martín-Rodríguez, R.; González, J. A.; Rodríguez, F.; Almonacid, G.; Segura, A.; Muñoz-Sanjosé, V.; Gamelin, D. R.; Valiente, R. Photoluminescence in Zno:Co2+ (0.01%−5%) Nanoparticles, Nanowires, Thin Films, and Single Crystals as a Function of Pressure and Temperature: Exploring Electron−Phonon Interactions. *Chem. Mater.* **2014**, *26*, 1100−1107.

(14) Zhuang, J.; Gao, N.; Li, Z.; Xu, X.; Wang, J.; Zhao, J.; Dou, S. X.; Du, Y. Cooperative Electron-Phonon Coupling and Buckled Structure in Germanene on Au(111). *ACS Nano* **2017**, *11*, 3553−3559.

(15) Faust, A.; Amit, Y.; Banin, U. Phonon-Plasmon Coupling and Active Cu Dopants in Indium Arsenide Nanocrystals Studied by Resonance Raman Spectroscopy. *J. Phys. Chem. Lett.* **2017**, *8*, 2519−2525.

(16) Siemens, M. E.; Li, Q.; Yang, R.; Nelson, K. A.; Anderson, E. H.; Murnane, M. M.; Kapteyn, H. C. Quasi-Ballistic Thermal Transport from Nanoscale Interfaces Observed Using Ultrafast Coherent Soft X-Ray Beams. *Nat. Mater.* **2010**, *9*, 26−30.

(17) Wang, Z.; Li, X.; Zhang, G.; Luo, Y.; Jiang, J. Suppressing Electron-Phonon Coupling through Laser-Induced Phase Transition. *ACS Appl. Mater. Interfaces* **2017**, *9*, 23309−23313.

(18) Guo, P.; Gong, J.; Sadasivam, S.; Xia, Y.; Song, T. B.; Diroll, B. T.; Stoumpos, C. C.; Ketterson, J. B.; Kanatzidis, M. G.; Chan, M. K. Y.; et al. Slow Thermal Equilibration in Methylammonium Lead Iodide Revealed by Transient Mid-Infrared Spectroscopy. *Nat. Commun.* **2018**, *9*, 2792.

(19) Qiu, T. Q.; Tien, C. L. Heat Transfer Mechanisms During Short-Pulse Laser Heating of Metals. *J. Heat Transfer* **1993**, *115*, 835−841.

(20) Long, R.; Prezhdo, O. V.; Fang, W. Nonadiabatic Charge Dynamics in Novel Solar Cell Materials. *Wiley Interdiscip. Rev. Comput. Mol. Sci.* **2017**, *7*, e1305.

(21) Hopkins, P. E.; Duda, J. C.; Kaehr, B.; Wang Zhou, X.; Peter Yang, C. Y.; Jones, R. E. Ultrafast and Steady-State Laser Heating Effects on Electron Relaxation and Phonon Coupling Mechanisms in Thin Gold Films. *Appl. Phys. Lett.* **2013**, *103*, 211910.

(22) Mueller, B. Y.; Rethfeld, B. Nonequilibrium Electron−Phonon Coupling after Ultrashort Laser Excitation of Gold. *Appl. Surf. Sci.* **2014**, *302*, 24−28.

(23) Govorov, A. O.; Zhang, H.; Demir, H. V.; Gun'ko, Y. K. Photogeneration of Hot Plasmonic Electrons with Metal Nanocrystals: Quantum Description and Potential Applications. *Nano Today* **2014**, *9*, 85−101.

(24) Heilpern, T.; Manjare, M.; Govorov, A. O.; Wiederrecht, G. P.; Gray, S. K.; Harutyunyan, H. Determination of Hot Carrier Energy Distributions from Inversion of Ultrafast Pump-Probe Reflectivity Measurements. *Nat. Commun.* **2018**, *9*, 1853.

(25) Garcia, G.; Buonsanti, R.; Runnerstrom, E. L.; Mendelsberg, R. J.; Llordes, A.; Anders, A.; Richardson, T. J.; Milliron, D. J. Dynamically Modulating the Surface Plasmon Resonance of Doped Semiconductor Nanocrystals. *Nano Lett.* **2011**, *11*, 4415−20.

(26) Mehdipour, H.; Smith, B. A.; Rezakhani, A. T.; Tafreshi, S. S.; de Leeuw, N. H.; Prezhdo, O. V.; Moshfegh, A. Z.; Akimov, A. V. Dependence of Electron Transfer Dynamics on the Number of Graphene Layers in Pi-Stacked 2d Materials: Insights from Ab Initio Nonadiabatic Molecular Dynamics. *Phys. Chem. Chem. Phys.* **2019**, *21*, 23198−23208.

(27) Guo, H.; Zhao, C.; Zheng, Q.; Lan, Z.; Prezhdo, O. V.; Saidi, W. A.; Zhao, J. Superatom Molecular Orbital as an Interfacial Charge Separation State. *J. Phys. Chem. Lett.* **2018**, *9*, 3485−3490.

(28) Giri, A.; Hopkins, P. E. Transient Thermal and Nonthermal Electron and Phonon Relaxation after Short-Pulsed Laser Heating of Metals. *J. Appl. Phys.* **2015**, *118*, 215101.

(29) Wang, W.; Lai, M.; Fang, J.; Lu, C. Au and Pt Selectively Deposited on {0 0 1}-Faceted Tio2 toward Spr Enhanced

Photocatalytic Cr(Vi) Reduction: The Influence of Excitation Wavelength. *Appl. Surf. Sci.* **2018**, *439*, 430−438.
(30) Yu, X.; Kim, B.; Kim, Y. K. Highly Enhanced Photoactivity of Anatase Tio2 Nanocrystals by Controlled Hydrogenation-Induced Surface Defects. *ACS Catal.* **2013**, *3*, 2479−2486.
(31) Zhou, Z.; Liu, J.; Long, R.; Li, L.; Guo, L.; Prezhdo, O. V. Control of Charge Carriers Trapping and Relaxation in Hematite by Oxygen Vacancy Charge: Ab Initio Non-Adiabatic Molecular Dynamics. *J. Am. Chem. Soc.* **2017**, *139*, 6707−6717.
(32) Olson, D. H.; Freedy, K. M.; McDonnell, S. J.; Hopkins, P. E. The Influence of Titanium Adhesion Layer Oxygen Stoichiometry on Thermal Boundary Conductance at Gold Contacts. *Appl. Phys. Lett.* **2018**, *112*, 171602.
(33) Kumar, A.; Sharma, V.; Kumar, S.; Kumar, A.; Krishnan, V. Towards Utilization of Full Solar Light Spectrum Using Green Plasmonic Au−Tiox Photocatalyst at Ambient Conditions. *J. Chem. Phys.* **2018**, *11*, 98−106.
(34) Li, W.; Zhou, L.; Prezhdo, O. V.; Akimov, A. V. Spin−Orbit Interactions Greatly Accelerate Nonradiative Dynamics in Lead Halide Perovskites. *ACS Energy Lett.* **2018**, *3*, 2159−2166.
(35) Craig, C. F.; Duncan, W. R.; Prezhdo, O. V. Trajectory Surface Hopping in the Time-Dependent Kohn-Sham Approach for Electron-Nuclear Dynamics. *Phys. Rev. Lett.* **2005**, *95*, 163001.
(36) Fischer, S. A.; Habenicht, B. F.; Madrid, A. B.; Duncan, W. R.; Prezhdo, O. V. Regarding the Validity of the Time-Dependent Kohn-Sham Approach for Electron-Nuclear Dynamics Via Trajectory Surface Hopping. *J. Chem. Phys.* **2011**, *134*, 024102.
(37) Wang, L.; Akimov, A.; Prezhdo, O. V. Recent Progress in Surface Hopping: 2011−2015. *J. Phys. Chem. Lett.* **2016**, *7*, 2100−12.
(38) Li, W.; Tang, J.; Casanova, D.; Prezhdo, O. V. Time-Domain Ab Initio Analysis Rationalizes the Unusual Temperature Dependence of Charge Carrier Relaxation in Lead Halide Perovskite. *ACS Energy Lett.* **2018**, *3*, 2713−2720.
(39) Tully, J. C. Molecular Dynamics with Electronic Transitions. *J. Chem. Phys.* **1990**, *93*, 1061−1071.
(40) Jaeger, H. M.; Fischer, S.; Prezhdo, O. V. Decoherence-Induced Surface Hopping. *J. Chem. Phys.* **2012**, *137*, 22A545.
(41) Wang, L. J.; Trivedi, D.; Prezhdo, O. V. Global Flux Surface Hopping Approach for Mixed Quantum-Classical Dynamics. *J. Chem. Theory Comput.* **2014**, *10*, 3598−3605.
(42) Trivedi, D. J.; Wang, L. J.; Prezhdo, O. V. Auger-Mediated Electron Relaxation Is Robust to Deep Hole Traps: Time-Domain Ab Initio Study of Cdse Quantum Dots. *Nano Lett.* **2015**, *15*, 2086−2091.
(43) Li, L. Q.; Lin, M. F.; Zhang, X.; Britz, A.; Krishnamoorthy, A.; Ma, R. R.; Kalia, R. K.; Nakano, A.; Vashishta, P.; Ajayan, P.; et al. Phonon-Suppressed Auger Scattering of Charge Carriers in Defective Two-Dimensional Transition Metal Dichalcogenides. *Nano Lett.* **2019**, *19*, 6078−6086.
(44) Kohn, W.; Sham, L. J. Self-Consistent Equations Including Exchange and Correlation Effects. *Phys. Rev.* **1965**, *140*, A1133−A1138.
(45) Akimov, A. V.; Prezhdo, O. V. The Pyxaid Program for Non-Adiabatic Molecular Dynamics in Condensed Matter Systems. *J. Chem. Theory Comput.* **2013**, *9*, 4959−72.
(46) Akimov, A. V.; Prezhdo, O. V. Advanced Capabilities of the Pyxaid Program: Integration Schemes, Decoherence Effects, Multi-excitonic States, and Field-Matter Interaction. *J. Chem. Theory Comput.* **2014**, *10*, 789−804.
(47) Chu, W.; Saidi, W. A.; Zheng, Q.; Xie, Y.; Lan, Z.; Prezhdo, O. V.; Petek, H.; Zhao, J. Ultrafast Dynamics of Photongenerated Holes at a Ch3oh/Tio2 Rutile Interface. *J. Am. Chem. Soc.* **2016**, *138*, 13740−13749.
(48) Li, L.; Long, R.; Prezhdo, O. V. Why Chemical Vapor Deposition Grown Mos2 Samples Outperform Physical Vapor Deposition Samples: Time-Domain Ab Initio Analysis. *Nano Lett.* **2018**, *18*, 4008−4014.
(49) Li, W.; Vasenko, A. S.; Tang, J.; Prezhdo, O. V. Anharmonicity Extends Carrier Lifetimes in Lead Halide Perovskites at Elevated Temperatures. *J. Phys. Chem. Lett.* **2019**, *10*, 6219−6226.
(50) Tong, C. J.; Li, L. Q.; Liu, L. M.; Prezhdo, O. V. Long Carrier Lifetimes in Pbi2-Rich Perovskites Rationalized by Ab Initio Nonadiabatic Molecular Dynamics. *ACS Energy Lett.* **2018**, *3*, 1868−1874.
(51) Zhang, Z.; Fang, W.-H.; Tokina, M. V.; Long, R.; Prezhdo, O. V. Rapid Decoherence Suppresses Charge Recombination in Multi-Layer 2d Halide Perovskites: Time-Domain Ab Initio Analysis. *Nano Lett.* **2018**, *18*, 2459−2466.
(52) Long, R.; Fang, W. H.; Prezhdo, O. V. Moderate Humidity Delays Electron-Hole Recombination in Hybrid Organic-Inorganic Perovskites: Time-Domain Ab Initio Simulations Rationalize Experiments. *J. Phys. Chem. Lett.* **2016**, *7*, 3215−3222.
(53) Long, R.; Prezhdo, O. V. Dopants Control Electron-Hole Recombination at Perovskite-Tio2 Interfaces: Ab Initio Time-Domain Study. *ACS Nano* **2015**, *9*, 11143−11155.
(54) Wang, L. J.; Long, R.; Prezhdo, O. V., Time-Domain Ab Initio Modeling of Photoinduced Dynamics at Nanoscale Interfaces. In *Annual Review of Physical Chemistry*; Johnson, M. A.; Martinez, T. J., Eds.; 2015; Vol. *66*, pp 549 ff.
(55) Yang, Y. T.; Fang, W. H.; Benderskii, A.; Long, R.; Prezhdo, O. V. Strain Controls Charge Carrier Lifetimes in Monolayer Wse2: Ab Initio Time Domain Analysis. *J. Phys. Chem. Lett.* **2019**, *10*, 7732−7739.
(56) Zhang, L. L.; Chu, W. B.; Zheng, Q. J.; Benderskii, A. V.; Prezhdo, O. V.; Zhao, J. Suppression of Electron-Hole Recombination by Intrinsic Defects in 2d Monoelemental Material. *J. Phys. Chem. Lett.* **2019**, *10*, 6151−6158.
(57) Zhou, G. Q.; Cen, C.; Wang, S. Y.; Deng, M. S.; Prezhdo, O. V. Electron-Phonon Scattering Is Much Weaker in Carbon Nanotubes Than in Graphene Nanoribbons. *J. Phys. Chem. Lett.* **2019**, *10*, 7179−7187.
(58) Li, W.; Long, R.; Tang, J. F.; Prezhdo, O. V. Influence of Defects on Excited-State Dynamics in Lead Halide Perovskites: Time-Domain Ab Initio Studies. *J. Phys. Chem. Lett.* **2019**, *10*, 3788−3804.
(59) Prezhdo, O. V.; Duncan, W. R.; Prezhdo, V. V. Photoinduced Electron Dynamics at the Chromophore-Semiconductor Interface: A Time-Domain Ab Initio Perspective. *Prog. Surf. Sci.* **2009**, *84*, 30−68.
(60) Zhou, X.; Jankowska, J.; Li, L.; Giri, A.; Hopkins, P. E.; Prezhdo, O. V. Strong Influence of Ti Adhesion Layer on Electron-Phonon Relaxation in Thin Gold Films: Ab Initio Nonadiabatic Molecular Dynamics. *ACS Appl. Mater. Interfaces* **2017**, *9*, 43343−43351.
(61) Long, R.; Prezhdo, O. V. Time-Domain Ab Initio Modeling of Electron-Phonon Relaxation in High-Temperature Cuprate Superconductors. *J. Phys. Chem. Lett.* **2017**, *8*, 193−198.
(62) Wang, Y.-S.; Zhou, X.; Tomko, J. A.; Giri, A.; Hopkins, P. E.; Prezhdo, O. V. Electron−Phonon Relaxation at Au/Ti Interfaces Is Robust to Alloying: Ab Initio Nonadiabatic Molecular Dynamics. *J. Phys. Chem. C* **2019**, *123*, 22842−22850.
(63) Jankowska, J.; Prezhdo, O. V. Real-Time Atomistic Dynamics of Energy Flow in an Stm Setup: Revealing the Mechanism of Current-Induced Molecular Emission. *J. Phys. Chem. Lett.* **2018**, *9*, 3591−3597.
(64) Liu, L.; Fang, W. H.; Long, R.; Prezhdo, O. V. Lewis Base Passivation of Hybrid Halide Perovskites Slows Electron-Hole Recombination: Time-Domain Ab Initio Analysis. *J. Phys. Chem. Lett.* **2018**, *9*, 1164−1171.
(65) Senanayake, R. D.; Guidez, E. B.; Neukirch, A. J.; Prezhdo, O. V.; Aikens, C. M. Theoretical Investigation of Relaxation Dynamics in Au38(Sh)24 Thiolate-Protected Gold Nanoclusters. *J. Phys. Chem. C* **2018**, *122*, 16380−16388.
(66) He, J.; Fang, W. H.; Long, R.; Prezhdo, O. V. Superoxide/Peroxide Chemistry Extends Charge Carriers' Lifetime but Undermines Chemical Stability of Ch3nh3pbi3 Exposed to Oxygen: Time-Domain Ab Initio Analysis. *J. Am. Chem. Soc.* **2019**, *141*, 5798−5807.

https://dx.doi.org/10.1021/acs.jpclett.9b03884
J. Phys. Chem. Lett. 2020, 11, 1419−1427

(67) Zhang, Z.; Fang, W. H.; Long, R.; Prezhdo, O. V. Exciton Dissociation and Suppressed Charge Recombination at 2d Perovskite Edges: Key Roles of Unsaturated Halide Bonds and Thermal Disorder. *J. Am. Chem. Soc.* **2019**, *141*, 15557−15566.
(68) Li, L.; Long, R.; Prezhdo, O. V. Charge Separation and Recombination in Two-Dimensional Mos2/Ws2: Time-Domain Ab Initio Modeling. *Chem. Mater.* **2017**, *29*, 2466−2473.
(69) Zhou, X.; Tokina, M. V.; Tomko, J. A.; Braun, J. L.; Hopkins, P. E.; Prezhdo, O. V. Thin Ti Adhesion Layer Breaks Bottleneck to Hot Hole Relaxation in Au Films. *J. Chem. Phys.* **2019**, *150*, 184701.

https://dx.doi.org/10.1021/acs.jpclett.9b03884
J. Phys. Chem. Lett. 2020, 11, 1419−1427